Divergence Instability and Diffuse Failure in Granular Media

Ali Daouadji, Mohamad Jrad, Florent Prunier, Luc Sibille, François Nicot, Farid Laouafa, Félix Darve

Available online at www.sciencedirect.com

SciVerse ScienceDirect

Procedia IUTAM 3 (2012) 115 – 140

Procedia IUTAM

www.elsevier.com/locate/procedia

Divergence Instability and Diffuse Failure in Granular Media

Ali DAOUADJI[a], Mohamad JRAD[a], Florent PRUNIER[b], Luc SIBILLE[c], François NICOT[d], Farid LAOUAFA[e], Félix DARVE[f]

[a]*Laboratoire d'Etude des Microstructures et de Mécanique des Matériaux - UMR CNRS 7239*
Université Paul Verlaine - Metz Ile du Saulcy57045 METZ cedex 1, France
[b]*Laboratoire de Génie Civil et Ingénierie Environnementale, Bâtiment Coulomb*
34 avenue des Arts, 69621 Villeurbanne cedex
[c]*Laboratoire GeM UMR CNRS - Université de Nantes, IUT de Saint Nazaire*
58, rue Michel-Ange - BP 420, 44606 Saint-Nazaire Cedex, France
[d]*Unité de Recherche Erosion Torrentielle Neige et Avalanches – Cemagref, Domaine Universitaire*
BP 76, F38402 - Saint Martin d'Hères Cedex - France
[e]*INERIS, Parc Technologique Alata, BP2, F-60550, Verneuil en Halatte, France*
[f]*Laboratoire Sols Solides Structures Risques, Institut Polytechnique Grenoble,*
BP 53 - 38041, Grenoble cedex 9 - France

Abstract

The question of divergence instability and diffuse failure, which is a common failure mode for granular materials like soils, is tackled here from an experimental, theoretical and numerical perspective. The necessary condition of instability as given by the loss of definite-positiveness of the elasto-plastic matrix (the so-called " second order work criterion") is considered to analyze some experimental tests leading to diffuse failure, the link between kinetic energy and second order work is established, a discrete element method is used to simulate these failure conditions and eventually a 3D bifurcation analysis is performed with incrementally piecewise and non-linear elasto-plastic relationships. Essentially in relation with the non-associate character of the plastic strains of granular materials, a whole bifurcation domain in the stress space emerges from these analyses, leading to novel views of failure for non-associative materials.

Keywords: instability; bifurcation; failure; kinetic energy; second order work; non associativeness

1. Introduction

It has been repeatedly observed that geomaterials (soils, rocks, concretes) can collapse under various failure modes, due to geometric or material instabilities. Material or constitutive instabilities can lead to localised (with plastic strain or damage localisation patterning) or diffuse failure (without any such pattern). Localisation appears in the form of shear bands ([1]), or less often with compaction/dilation

 doi:10.1016/j.piutam.2012.03.009

bands. Diffuse failure modes by divergence instability correspond to the case where the soil collapses *in situ* into a shapeless body with a random displacement field, showing no internally organised strain structure ([2]). This kind of failure is observed in nature for example after strong rainfalls or after an earthquake in the case of the liquefaction of loose saturated sands. Even though viscosity plays an important role in clay collapse (typically by tertiary creep), the purpose of this paper will be restricted to the case of rate-independent geomaterials.

The first section of this paper is devoted to the observation and analysis of such diffuse failure modes in lab experiments performed in axisymmetric conditions with a triaxial apparatus on a loose sand. Various strain proportional loading paths are considered to investigate the influence of the loading direction on the occurrence of failure.

If flutter instabilities are excluded, the necessary condition for diffuse or localised failure is given by the second order work criterion, which corresponds to the loss of definite positiveness of the elasto-plastic operator (or equivalently of its symmetric part). One crucial point here is that geomaterials are strongly non-associative materials, characterised by a dilatancy angle different from the friction angle. Thus the elasto-plastic operator is non-symmetric and the second order work criterion (related to the singularity of the symmetric part of the elasto-plastic matrix) is essentially different from the plastic limit condition (singularity of the elasto-plastic matrix itself). Moreover, linear algebra shows that the second condition is met after the first one (along a given loading path), giving rise to the existence of a whole bifurcation domain in the stress space limited by both the determinants of the elasto-plastic matrix and its symmetric part vanishing respectively.

A question appears now: what is the essential link between second order work criterion and failure? This is the object of the second section, where this link is emphasized through a relationship between the kinetic energy at and just after failure as a function of the difference between the external second order work corresponding to the applied loading at the body boundary and the internal second order work of the deformed body. For quasi-static conditions far from failure, this difference is nil, the kinetic energy is thus equal to 0 and the medium remains in an equilibrium static case. At failure, because of the vanishing of second order work, the kinetic energy can take finite positive values (for proper applied loading parameters) giving rise to bursts of kinetic energy leading to failure. The stress-strain state reaches a limit state (which can be a mixed one as seen in section 4). On the other hand, effective failure is associated with large strains suddenly developing in a dynamic regime.

Having observed these bursts of kinetic energy at specimen collapse in experiments, and having established the link between kinetic energy and failure, it is interesting =to analyse these collapses by direct numerical simulations. This is the purpose of Section4, where discrete element simulations of axisymmetric triaxial tests are performed. A discrete element model (DEM) is used which is, roughly speaking, the application of molecular dynamics to granular materials. DEM is currently used now in geomechanics, since its capability to produce very realistic results has been checked in the past in a very detailed way ([3], [4] and [5]). The relationship between second order work and kinetic energy is thus very carefully examined and discussed.

Then in the last and fifth section, a 3D bifurcation analysis is performed by considering both an incrementally piece-wise linear and an incrementally non-linear rate-independent constitutive relation. The boundaries of the bifurcation domain are given in 3D for Hostun sand. As the second order work corresponds to the quadratic form associated with the elasto-plastic matrix, this form takes negative values inside “the isotropic cone” of this matrix according to linear algebra. Thus, from a mechanical point of view, the second order work has negative values inside some “instability cones”, providing the “unstable loading directions” which can lead to failure by divergence instability if proper loading parameters are considered. These cones are presented for general 3D loading conditions.

2. Experimental behavior of loose granular materials under axisymmetric proportional strain tests

The behaviour of granular materials has been mostly studied in laboratories using compression or extension triaxial tests carried out on saturated samples under either fully drained or fully undrained conditions. This practice is considered appropriate since drained and undrained behaviour are supposedly the bounds of all possible material behaviour under saturated conditions. However, in the case of saturated materials, the real *in situ* conditions are in fact partially drained which means a simultaneous change in both pore volume and pore-water pressure. The mechanical behaviour of a given soil depends on its current state (related to its deposition and loading history), the external loading and the rate of loading (for rate sensitive materials), its permeability and of course on the boundary conditions. Indeed, five types of drainage for saturated granular materials can be considered as follows: excessive drainage, full drainage, partial drainage, zero drainage and expansive drainage. The full and zero drainage conditions are equivalent respectively to classical drained and undrained tests. Partial drainage corresponds to a volumetric deformation bounded by the drained and undrained volumetric deformations (nil for the latter), that is representative of coarse soils subjected to rapidly changing loads. The last two types of drainage conditions can be observed when the pore pressure at the boundary is different from that inside the element of interest. If higher surrounding pore pressure exists, then pore-water will flow into the soil causing expansive drainage of the considered domain. On the other hand, a lower pore pressure applied at boundary will draw water out of the element of soil and lead to a greater volume contraction than the contraction observed during full drainage. Indeed, for the latter the pore water pressure remains constant and does not decrease. To experimentally obtain these five drainage conditions with the conventional triaxial setup, several authors have used the proportional strain path tests by imposing a constant strain ratio $\alpha = d\varepsilon_v/d\varepsilon_1$, where $d\varepsilon_v = d\varepsilon_1 + 2\, d\varepsilon_3$ ([6], [7], [8] and [9]).

In partCUlar, instability was studied under axisymmetric undrained compression tests or constant-q tests (See[10], [11] and [12] for more details) and the role of the control parameters on the effective collapse was emphasised using the approach proposed by R. Nova ([13]). In this Section, experimental results obtained during three undrained triaxial compression tests and four proportional strain tests on saturated sand are presented.

2.1. Tested material and physical model

Tests were performed on Hostun S28 sand, which is a sub-angular, medium sand (see Table 1). In order to obtain the loosest collapsible samples, the moist tamping method was adopted for the preparation of the samples. Dry sand was mixed with approximately 3% of de-aired water and then deposited in a mould in five layers. Each layer was compacted using a tamper to reach the same-targeted height after compaction. Then, the enlarged platens was coated with a thin layer of lubricant in order to reduce the friction with the soil at the top and bottom of the samples. Saturation was achieved by first flushing carbon dioxide and then de-aired water under a very low pressure (less than 10 kPa). Finally, the saturation process was stopped after the Skempton's B-parameter was greater than 98%.

Table 1: Basic properties of Hostun S28 sand ([10])

Type	Mean Size (mm)	Uniformity coefficient	Specific gravity	Max void ratio	Min void ratio	Frictional angle (°)
Quartzic	0.3–0.35	2	2.65	1	0.656	32

A triaxial cell was used in combination with an electromechanical compression and traction testing machine. The cell pressure was applied through a digital pressure-volume controller (DPVC). A second DPVC device was used to apply the backpressure and to measure volume variation at the bottom of the specimen (or to measure the backpressure and to apply the volume variation respectively). The load applied using the loading frame was measured using a submergible force transducer placed inside the cell in contact with the sample. The axial displacements were obtained using a transducer placed inside the compression traction-testing machine. All data were recorded on a computer, which was also used to impose the desired loading path.

2.2. Loading program

2.2.1. Undrained triaxial compression tests

During an undrained triaxial compression test, the prescribed loading program is given by the following conditions:

$$\begin{cases} d\varepsilon_1 > 0 \text{ or } dq > 0 \\ d\sigma'_2 = d\sigma'_3 \\ d\varepsilon_v = 0 \end{cases} \quad (1$$

where $q = \sigma_1 - \sigma_3$

As the sample is saturated, the isochoric condition (no volume variation) is imposed at the boundary and the pore water pressure evolves depending on sample density. For loose samples, the pore water pressure continuously increases up to a plateau whereas for a denser sample, it increases to a peak and then decreases. During the tests, the total (external) radial stress applied is maintained constant. The sample can be loaded under a strain-controlled or stress controlled mode (Equation 1).

2.2.2. Axisymmetric strain proportional tests

During an imposed axisymmetric strain proportional test, the loading program is described by the following conditions:

$$\begin{cases} d\varepsilon_1 > 0 \\ d\varepsilon_2 = d\varepsilon_3 = cst \\ \alpha = \dfrac{d\varepsilon_v}{d\varepsilon_1} \end{cases} \quad (2$$

with the common sign convention used in geomechanics, where axial compression and volume outflow are considered as positive. Therefore a positive α value corresponds to a volumetric contraction whereas a negative α value corresponds to a volumetric expansive deformation. Following the value and the sign of the parameter α the test is either:

- $\alpha = 0$: undrained test (or zero drainage),
- $\alpha > 0$: contractive test (equivalent to partial or excessive drainage following α value),
- $\alpha < 0$: expansive (or dilative) test,

It should be noticed that $\alpha = 1$ corresponds to a one-dimensional test.

Although the *in situ* conditions are clearly different, a constant strain ratio has been chosen during the whole test to study the influence of drainage condition on the instability of loose saturated Hostun sand. Similar tests have been performed by Lancelot et *al*. ([7]) and Sivathayalan and Logeswaran ([8]). Darve et *al*. ([14]) have used an equivalent definition of the proportional strain paths in order to numerically investigate such tests. The loading program is written in the following form

$$\begin{cases} d\varepsilon_1 > 0 \\ d\varepsilon_2 = d\varepsilon_3 = cst \\ d\varepsilon_1 + 2Rd\varepsilon_3 = 0 \end{cases} \quad (3$$

It can easily be shown that the parameters α and R are related by the following relation:

$$\alpha = 1 - \frac{1}{R} \quad (4$$

It follows that:

- $0<R<1$ produces an expansive imposed path,
- $R=1$ corresponds to an undrained path,
- $R>1$ produces a contractive path,
  and $R>>1$ corresponds to a one-dimensional test.

2.3. Experimental results

2.3.1. Undrained triaxial compression tests

Experimental tests on loose saturated samples loaded under strain-controlled mode (CU 1 and CU2) and stress-controlled mode (CU3) are performed for two effective mean stresses p'_0=100 and 300 kPa and results are plotted in Figure 1. Figure 1 shows the influence of the effective mean stress on the deviatoric stress. It is shown that a peak stress is reached for loose sands irrespective of the effective mean stress. The comparison between CU2 and CU3 shows a very good agreement for the axial strain and the deviatoric stress. But while the loading program can be followed to large strain well after the peak for the strain-controlled test (CU2), it is not possible to maintain the loading program at this point for the stress-controlled test (CU3). A dramatic drop in the deviatoric stress and a sudden increase in the axial strain is observed. The failure is effective for the latter but not for the former.

2.3.2. Axisymmetric strain proportional tests

Experimental data on loose saturated samples loaded under four proportional strain paths performed for one effective mean pressure p'_0=100 kPa are plotted in Figure 2. Different values of the parameter R corresponding to expansive (R=0.68), undrained (R=1) and contractive (R=1.36 and 2) volumetric strains were applied. Figure 2.c presents a linear variation of the volumetric strain plotted against the axial strain, which corresponds to the desired linear proportional path (see Eq. 2). Following the desired value of the R parameter, the deviatoric stress q could present a peak or not as shown in Figure 2.a. The observed peaks are followed by a total loss of strength (vanishing of the deviatoric stress) for values of R lower than or equal to 1 or a partial loss of strength for R=1.36. It should be emphasised that for R=2, no peak was observed and high strength mobilization can be reached at the end of the test. It is also observed in Figure 2.a that the peak values of the deviatoric stress q decreases with an increase in the expansive rate i.e. for decreasing values of R. The minimum q peak value reached during an expansive proportional strain path (R=0.68) is smaller than the one reached during conventional undrained test (R=1).

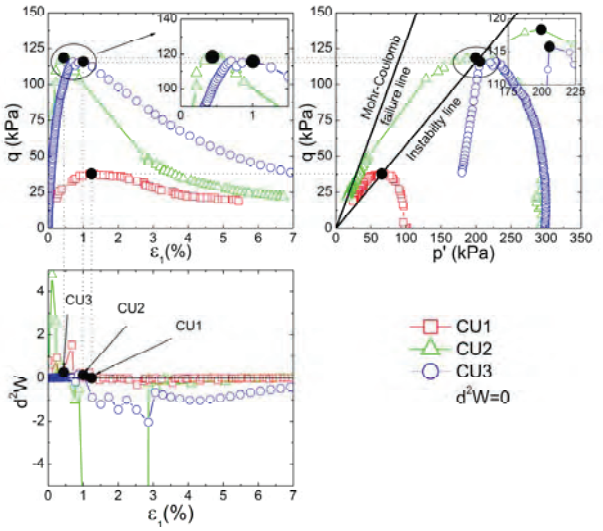

Figure 1. Experimental results of undrained triaxial compression tests on loose Hostun sand. The initial effective mean stresses are p'_0 = 100 and 300 kPa.

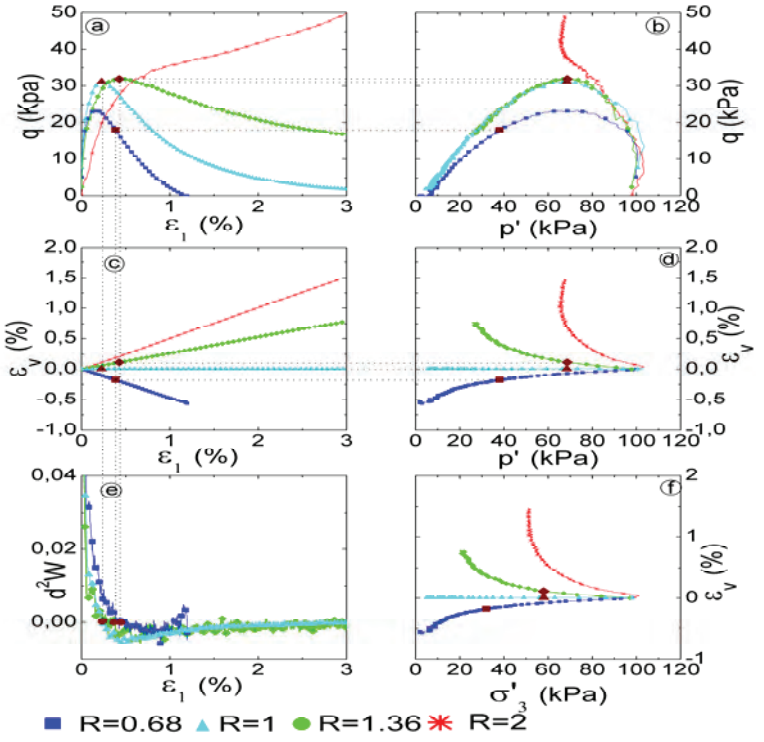

Figure 2. Experimental results of axisymmetric proportional strain tests on loose Hostun sand. The initial effective mean stresses p'_0 is100 kPa and four different values of R were imposed (0.68, 1, 1.36 and 2).

3. Instability, failure and kinetic energy

Let us come back first to some basic definitions. In the approach presented in this chapter, the mechanical (stress-strain) state of a given material system, after a given loading history, is unstable if the kinetic energy of the system increases due to infinitesimal loading (disturbance). In partCUlar, if the system is initially at rest and at equilibrium under external forces, an increase in kinetic energy means that there is a transition from a quasistatic regime towards a dynamic regime. This transition is basically a bifurcation.

The dynamic regime may usually lead to the collapse of the system, and corresponds therefore to an effective failure, that can be localized (a localization pattern develops) or diffuse (the kinematic field remains chaotic, without specific localization). This is what is observed from experimental tests: considering an undrained or an expansive strain proportional triaxial test applied to (loose) sand specimen, the deviatoric stress is known to reach a maximum and then to decrease. After the peak, if an additional deviatoric load is applied (together with the isochoric condition), then the specimen abruptly fails with a clear evidence of outbursts in kinetic energy (CU3 test of Section 2).

In conclusion, instability of a mechanical state may lead to an increase in kinetic energy (which is a clear evidence of failure), depending on some imperfections, disturbances, etc. In the following paragraph, we investigate the conditions under which the kinetic energy of the system may increase.

For a material system made up of a volume V_o, initially in a configuration C_o of boundary (Γ_o), in equilibrium at time *t* under a prescribed external loading, it was established that the second-order time differentiation of the kinetic energy (at time *t*) written in Lagrangian formulation ([15]; and [16]):

$$\delta^2 E_c(t) = \int_{\Gamma_o} \delta f_j \; \delta u_i \; dS_o - \int_{V_o} \delta \Pi_{ij} \; \frac{\partial(\delta u_i)}{\partial X_j} \; dV_o \tag{5}$$

where $\overline{\overline{\Pi}}$ denotes the Piola-Kirchoff stress tensor of the first kind and $\bar{f}$ the current forces applied to the initial (reference) configuration. Equation (5) introduces explicitly the second-order work that expresses through a semi-Lagrangian formalism as:

$$W_2 = \int_{V_o} \delta \Pi_{ij} \; \frac{\partial(\delta u_i)}{\partial X_j} \; dV_o \tag{6}$$

where $\delta \bar{u}$ denotes the current incremental displacement of the material points initially located at the position $\bar{X}$.

In addition, the two-order Taylor expansion of kinetic energy reads as:

$$E_c(t+\Delta t) = E_c(t) + \Delta t \; \dot{E}_c(t) + \frac{(\Delta t)^2}{2} \ddot{E}_c(t) + o(\Delta t)^3 \;\; (\forall \; \Delta t) \tag{7}$$

Noting that $E_c(t) = \int_{V_o} \rho_o \left\| \dot{\vec{u}} \right\|^2 dV_o$, where ρ_o is the density of the material in the initial configuration at point $M(\vec{X})$, since the system is in an equilibrium state at time t, then $E_c(t) = 0$. Furthermore, $\dot{E}_c(t) = \int_{V_o} \rho_o \, \dot{\vec{u}} \cdot \ddot{\vec{u}} \, dV_o$, and at time t, $\dot{E}_c(t) = 0$. Thus, ignoring third-order terms, Eq. (7) reads

$$\delta^2 E_c(t) = 2E_c(t + \delta t) \tag{8}$$

In combination with Eqs. (5) and (6), it follows that:

$$2E_c(t + \delta t) = \int_{\Gamma_o} \delta f_j \, \delta u_i \, dS_o - W_2 \tag{9}$$

As a consequence, the increase of kinetic energy for a material system initially in equilibrium (at rest) equals to the difference between a second-order boundary term (that involves the displacements and the forces acting on the boundary) and the so-called second-order work (built from the internal stress and strain acting in each point of the system). While the boundary term is related to the external loading, the second-order work is intimately related to the constitutive behavior of the material ([17]).

It is worth noting that two situations are of interest, that lead to a subsequent positive value of the kinetic energy from an equilibrium state: (1) the loading is controlled such that the boundary integral $\int_{\Gamma_o} \delta f_j \, \delta u_i \, dS_o$ becomes strictly larger that W_2 ; and (2) the boundary integral is kept nil, while the loading direction is such that W_2 is strictly negative. It can be shown that both are related to a conflict between the internal forces (resulting from the internal stress) applied to the interior of the boundary, and the external forces (imposed by the operator or any other external action) applied to the exterior of the boundary ([17]). It can be seen in Figure 1 and Figure 2.e that the peak of the deviatoric stress corresponds to the vanishing of the second order work during undrained tests and is negative during the descending branch. Its value can be positive during the descending branch in the *q*-p' or *q*-ε_1 planes for strain proportional test as the variables are not the proper conjugated control variables as defined in Section 5.

4. Simulation of effective failure with a discrete element model

This section is devoted to the investigation of the increase in the kinetic energy when effective failure is triggered from an equilibrium state. In partCUlar, we will focus on the relationship between the kinetic energy and the balance between the second-order work and the second-order boundary term as defined in Equation 9.

4.1. Set up of numerical experiments

We consider a system composed of a granular assembly of purely frictional spheres constituting a

representative elementary volume. In order to be able to follow the kinetic energy and the balance between internal forces (resulting from internal stresses) and external forces (imposed on the exterior of the boundaries of the considered sample), this investigation is performed from direct simulations based on the discrete element method ([18]). In such methods, inertial terms are taken into account and the motion of each particle within the granular assembly results directly from the explicit time integration of dynamic fundamental equations.

The granular assembly considered here has an initial cubical shape and is surrounded by six frictionless walls delimiting the six faces of the sample (Fig. 3). Principal directions of average stress and strain coincide with the normal directions to the walls. Hence, stress or strain boundary conditions (in terms of principal stress and strain components) can be imposed by controlling the six walls surrounding the sample. A boundary strain is prescribed by simply adjusting wall positions. In the case of a stress control at the boundary with respect to the direction *I*, walls are considered as dynamic objects and are submitted to an external normal force F_i^{ext}. Walls will then translate (rotation is locked) according to Newton's second law, until F_i^{ext} is balanced by reaction of the granular assembly on walls.

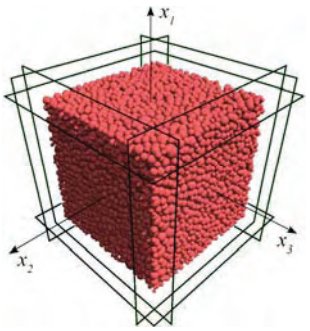

Figure 3 The cubical granular assembly composed of 10,000 spheres and enclosed with six walls

For the sake of simplicity, the analysis of numerical data is carried out in an Eulerian formalism. In addition, only average strain state and average stress state of the granular assembly is assessed based on a sample homogeneity approximation. In these conditions, the second-order work reads:

$$W_2 = V\,\delta\sigma_i\,\delta\varepsilon_i \tag{10}$$

where:

- σ_{ij} is the average internal Cauchy stress state computed with the Love-Weber formula ([19] and [20]):

$$\sigma_{ij} = \frac{1}{V}\sum_{contacts} r_i^c\, l_j^c \tag{11}$$

with $\vec{r}^{\,c}$ the inter-particle contact force and $\vec{l}^{\,c}$ the branch vector joining the center of the two particles involved in the contact,

- ε_{ij} is the average strain computed from positions of walls.

The external stress distribution s_i applied at the boundary of the granular assembly on a wall of normal i is simply deduced from the reaction force F_i of the sample on this wall (equal to the sum of the sphere-wall contact forces): $s_i = F_i / A_i$, where A_i is the current area of the face of normal i of the sample. When the sample is force-controlled in direction i, s_i can also be determined as $s_i = F_i^{ext} / A_i$, where F_i^{ext} is the external force applied on the wall[1].

By taking into account these variables, Equation 10, stating the increase of kinetic energy for the sample initially at rest, writes:

$$2E_c(t+\delta t) = V\,\delta s_i\,\delta\varepsilon_i - W_2 \tag{12}$$

where W_2 is computed here as defined in equation 9.

4.2. Numerical granular assemblies and quasi-static response

In the following, the development of effective failure in terms of kinetic energy is investigated for two different loading conditions and two numerical samples. We consider the case of drained triaxial compression on a dense sample and the case of an isochoric triaxial compression on a loose sample. Characteristics of numerical samples are given in Table 2. They are composed of 10,000 spherical particles (see Figure 3) interacting through a purely frictional contact law, characterized by normal and tangential stiffnesses (respectively k_n and k_t) and a friction angle φ_c in the tangential contact direction.

Table 2: characteristics of numerical samples under an isotropic confinement pressure of 100 kPa

.Sample	Porosity n	Coordination number z	k_n / D_S (MPa) (D_S : sphere diameter)	k_t / k_n	φ_c (deg.)
Dense	0.387	4.53	250	0.5	35
Loose	0.403	3.55	250	0.5	35

[1] Determination of the external stress distribution s_i from F_i or F_i^{ext} is equivalent if wall inertia is sufficiently small, otherwise a significant delay between changes of F_i and F_i^{ext} can be observed.

Both samples are compressed from an isotropic stress state of 100 kPa. For the dense sample, the radial external stresses s_2 and s_3 are kept constant and equal to 100 kPa while a constant axial strain rate $\dot{\varepsilon}_1$ = 0.01s^{-1} is imposed. Simulated response is displayed in Figure 4 in terms of internal σ_1 and external s_1 axial stresses, and porosity versus axial strain. Along this drained triaxial path and for this mode of control, effective failure does not occur: at any time, the prescribed forces applied at the boundary are balanced by internal stresses developed by the granular assembly itself.

The loose sample is compressed by imposing $\dot{\varepsilon}_1$ = 0.01 s^{-1} in the axial direction while positions of walls in directions '2' and '3' are adjusted at any time to follow the kinematic condition defined by $\dot{\varepsilon}_2 = \dot{\varepsilon}_3 = -\dot{\varepsilon}_1/2$, such that the isochoric condition $\dot{\varepsilon}_V = \dot{\varepsilon}_1 + \dot{\varepsilon}_2 + \dot{\varepsilon}_3 = 0$ is satisfied, which corresponds to R = 1 in Section 2. We define from the average external stresses and the average internal stresses respectively, the external deviatoric stress $q_s = s_1 - s_3$, and mean pressure $p_s = (s_1 + s_2 + s_3)/3$; and the internal deviatoric stress $q_\sigma = \sigma_1 - \sigma_3$ and mean pressure $p_\sigma = (\sigma_1 + \sigma_2 + \sigma_3)/3$. Once again, in this case where effective failure (with a deviation of the response from a quasi-static one to a dynamic one) is not triggered, average stress states computed at the boundary of the sample or from the Love-Weber formula are identical, as displayed in Figure 5 in the $q_s - p_s$ and $q_\sigma - p_\sigma$ plane for instance. Figure 5 shows that, after reaching a maximum deviatoric stress, stresses vanish and the sample liquefies. However local peaks of q_s (or q_σ) during the liquefaction phase suggests that the granular assembly recovers strength temporarily and the sample is at the very limit of liquefaction under the isochoric condition.

4.3. Investigation of effective failure

For both dense and loose samples, effective failure can be triggered by changing the mode of control of the samples from stress-strain states reached along the drained and undrained compression paths respectively ([21]).

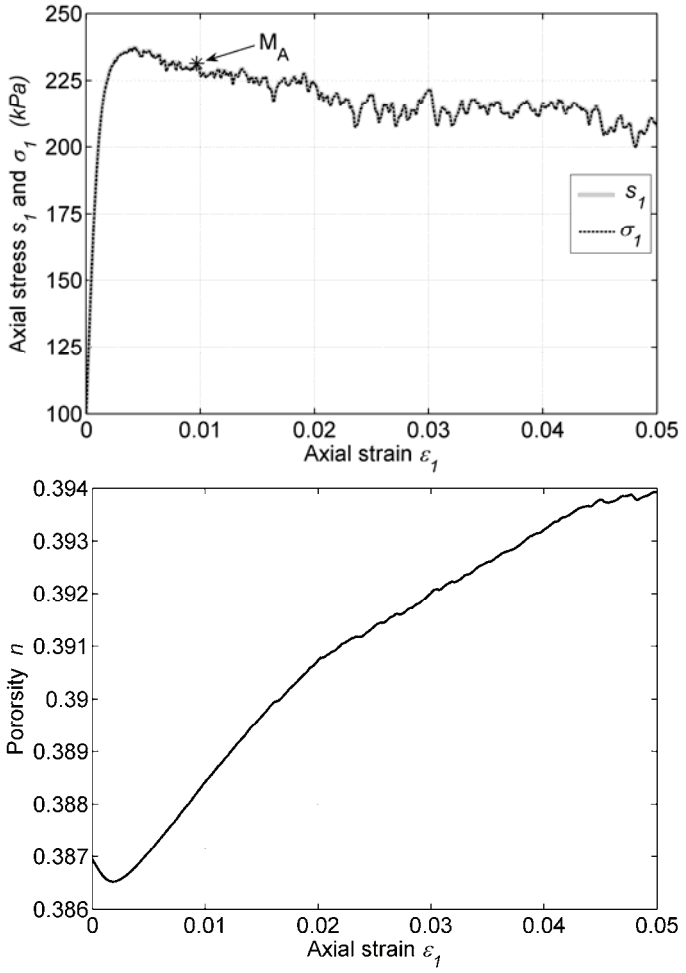

Figure 4. Drained triaxial compression on the dense sample for a confinement pressure of 100 kPa, internal σ_1 and external s_1 axial stresses are here equal.

For the dense sample, the state M_A represented in Figure 4 after the peak of s_1 (or σ_1) and characterized by $s_1^{M_A} = \sigma_1^{M_A}$ = 231.3 kPa is considered. At this state, the control at the boundary of the sample is switched to a full stress control by imposing $s_1 = s_1^{M_A}$ = 231.3 kPa and s_2 = s_3 = 100 kPa, until the sample stabilizes under the prescribed external stress state. Then a small stress increase is imposed at the boundary of the sample in the axial direction and defined by Δs_1 = 2 kPa (representing less than 1 % of $\sigma_1^{M_A}$), while the boundary conditions in the radial directions are still unchanged (s_2 = s_3 = 100 kPa). Change of axial stresses, in terms of external stress increment Δs_1 and internal stress increment $\Delta\sigma_1$ with respect to the stress state M_A, is displayed in Figure 6.

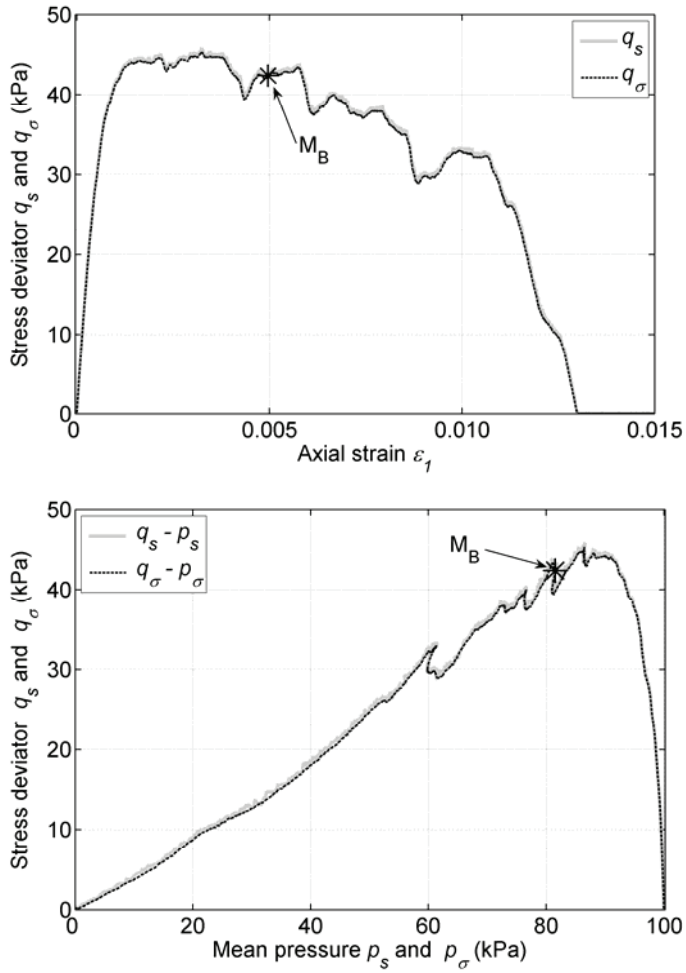

Figure 5. Undrained (isochoric) triaxial compression on the loose sample, internal average stress state ($q_\sigma - p_\sigma$) and average stress state computed at the boundary of the sample ($q_s - p_s$) are here identical.

The increase in the axial stress imposed at the boundary over a short time range is observable during the first 0.01 s, it is then kept constant and equal to the prescribed value of 2 kPa. The internal axial stress σ_1 increases at first (due to low additional strength acquired during the previous stabilization stage), but then rapidly decreases diverging from the axial stress prescribed at the boundary of the sample. For the loading program considered here, the granular assembly is not able to balance the external forces applied at its boundaries, and consequently, kinetic energy[2] increases monotonously as shown in Figure 7.

[2] The kinetic energy is computed as the sum of the translational and rotational kinetic energy of all the particles constituting the granular assembly.

In Figure 7 are also presented time series of $[W_2]_{\Delta t}$, $[V\,\Delta s_i \Delta \varepsilon_i]_{\Delta t}$, and $[(V\,\Delta s_i \Delta \varepsilon_i - W_2)/2]_{\Delta t}$ computed over a time increment Δt ranging from the application time of Δs_1 to the current time. The negative sign of the second-order work W_2 is related to negative values of $\Delta \sigma_1$ whereas $\Delta \varepsilon_1$ is positive. The boundary term $V\,\Delta s_i \Delta \varepsilon_i$ is positive since $\Delta s_1 > 0$. For time increments Δt < 0.05 s a rather good agreement is found between the kinetic energy and $[(V\,\Delta s_i \Delta \varepsilon_i - W_2)/2]_{\Delta t}$ as expected from Equations 12 and 9. Indeed these relationships (Equations 12 and 9) hold for an infinitesimally small time increment δt from an initial equilibrium state, but fail at large time increments for which Equation 8 is no longer valid.

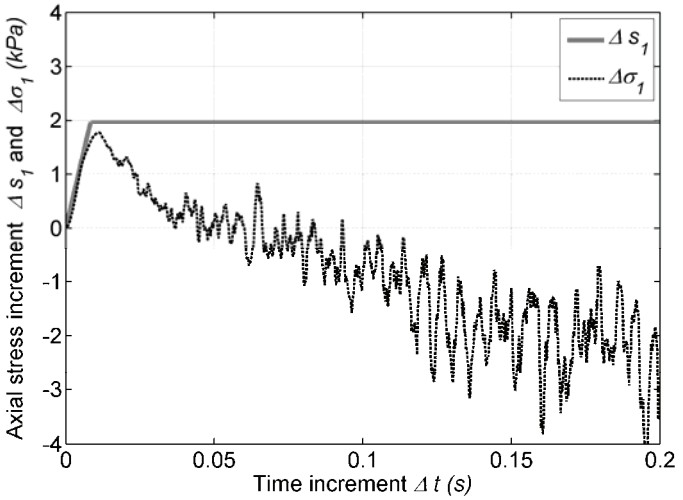

Figure 6. Incremental changes of external stress Δs_1 and internal stress $\Delta \sigma_1$, from the equilibrium state M_A, during and after the application of Δs_1 = 2 kPa.

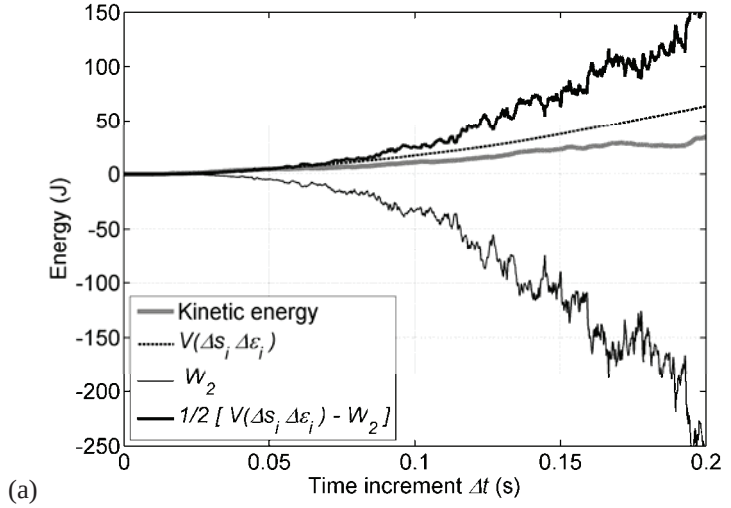

(a)

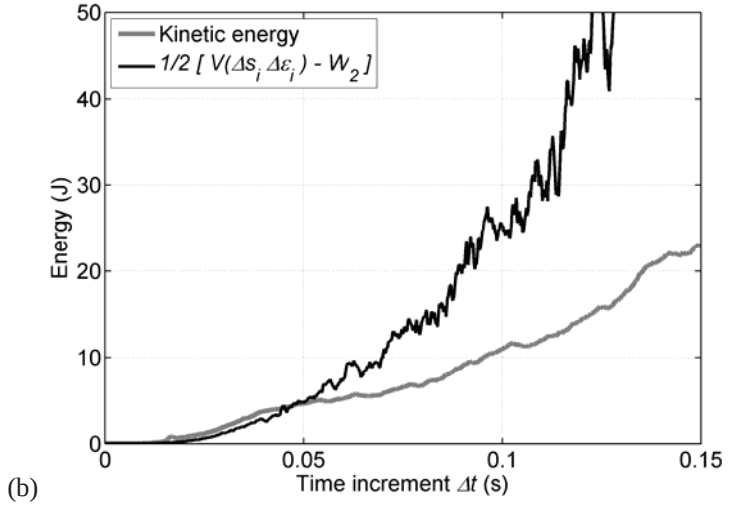

(b)

Figure 7. a) Time series of kinetic energy and second-order work $[W_2]_{\Delta t}$, boundary term $[V\,\Delta s_i \Delta\varepsilon_i]_{\Delta t}$ and $[(V\,\Delta s_i \Delta\varepsilon_i - W_2)/2]_{\Delta t}$ computed over time increments Δt running from the time of application of Δs_1 = 2 kPa from the equilibrium state M_A ; b) zoom on short time increments.

A process similar to the previous one is followed for the loose sample loaded in an isochoric condition. The granular assembly is first stabilized at the state M_B indicated in Figure 5 after the peak of q_s (or q_σ). The sample control is switched from strain control to stress control by prescribing the deviatoric stress deviator $q_s = q_s^{M_B}$ = 43 kPa at the sample boundary, while the isochoric condition $\dot{\varepsilon}_2 = \dot{\varepsilon}_3 = -\dot{\varepsilon}_1/2$ is still imposed ([22]). After this stabilization stage, a small additional deviatoric

stress Δq_s = 1.6 kPa (about 3.7 % of $q_s^{M_B}$) is applied at the boundaries. Increments of external and internal deviatoric stresses from the equilibrium state M_B are shown in Figure 8. As observed for drained compression, the sample is not able to develop internal stresses to balance the loading applied at its boundaries, while the isochoric condition is maintained. As effective failure develops, the boundary term $[V\,\Delta s_i \Delta \varepsilon_i]_{\Delta t}$, computed over time increments Δt, takes positive values while the second-order work $[W_2]_{\Delta t}$ becomes negative, leading to increasing values of kinetic energy (see Figure 9). Finally, kinetic energy and $[(V\,\Delta s_i \Delta \varepsilon_i - W_2)/2]_{\Delta t}$ are in agreement for time increments smaller than 0.08 s (Figure 9, not too far from the threshold found for the dense sample in drained condition).

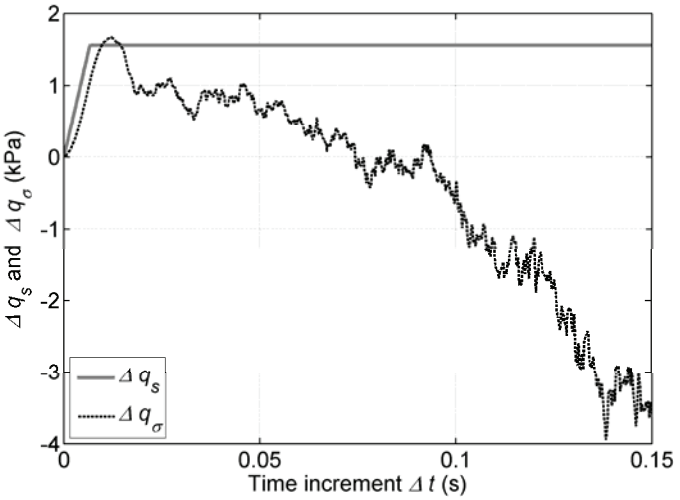

Figure 8. Incremental changes of external deviatoric stress Δq_s and internal deviatoric stress Δq_σ, from the equilibrium state M_B, during and after the application of Δq_s = 1.6 kPa.

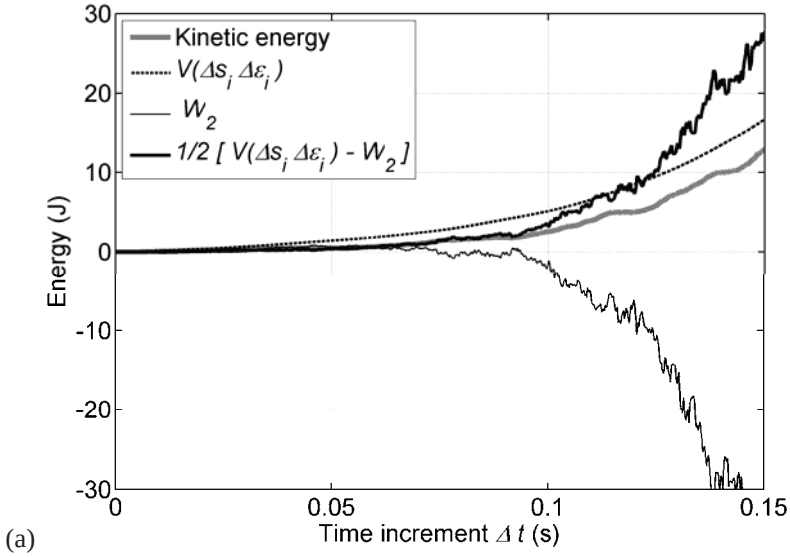

(a)

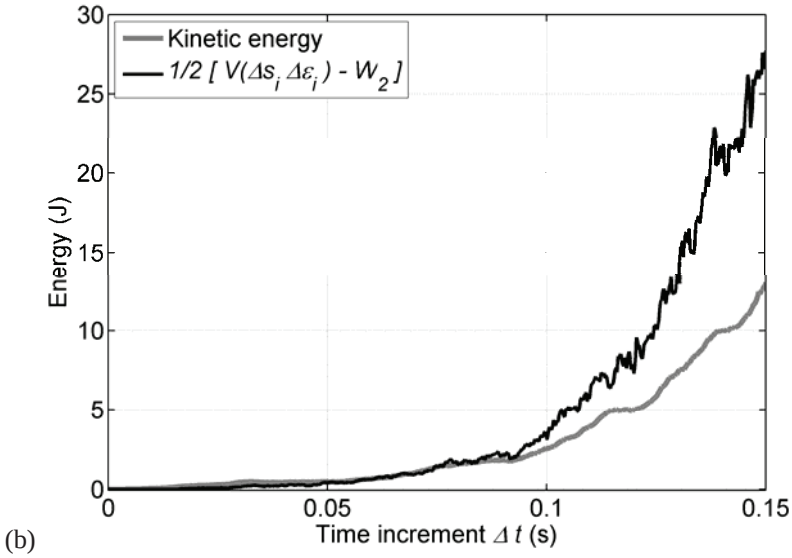

(b)

Figure 9. a) Time series of kinetic energy and second-order work $[W_2]_{\Delta t}$, boundary term $[V\,\Delta s_i \Delta\varepsilon_i]_{\Delta t}$ and $[(V\,\Delta s_i \Delta\varepsilon_i - W_2)/2]_{\Delta t}$ computed over time increments Δt running from the time of application of Δq_s = 1.6 kPa from the equilibrium state M_B ; b) zoom on short time increments.

5. Material stability criterion or divergence instability criterion for rate independent materials

Basically, failure in elasto-plastic media is defined with a limit stress state. Nevertheless, it is now well established that localized failure modes such as shear band or diffuse failure modes at collapse without localized patterns can arise strictly inside the plasticity limit when considering non-associated materials ([13], [23] and [24]). As discussed in Section 3, in the case where the boundary integral of Equation 8 is kept nil at the bifurcation point (for example by dead loads), effective failure accompanied with development of kinetic energy can occur only if the second order work becomes negative. Therefore, in a local form and in an Eulerian formalism with negligible geometrical effects (as done in Section 4), a sufficient condition of stability can be written is the following way ([25]):

$$\forall \left(\underline{\underline{d\sigma}}, \underline{\underline{d\varepsilon}}\right) \quad d^2W = \underline{\underline{d\sigma}} : \underline{\underline{d\varepsilon}} > 0 \tag{13}$$

where $\underline{\underline{d\sigma}}$ is the Cauchy stress rate tensor, and $\underline{\underline{d\varepsilon}}$ the small strain rate tensor. It is worth noting that the converse is generally false. Thus this expression gives a sufficient stability condition.

5.1. Basic analysis of second order work criterion

In this section only rate independent materials are considered. As a consequence, the constitutive relation takes the following form:

$$\underline{\underline{F_h}}\left(\underline{\underline{d\sigma}}, \underline{\underline{d\varepsilon}}\right) = 0 \tag{14}$$

$\underline{\underline{F_h}}$ is a non linear function depending on the state and history parameters $\underline{h}$. Nevertheless, in classical elasto-plasticity theory function $\underline{F_h}$ is piece wise linearized. In most basic theory, an elastoplastic tensor is defined for loading and another elastic one for unloading. In the following paragraph we will denote the tensorial zone a part of the incremental loading space for which the constitutive relation is linear. A tensorial zone is a generalization of the notion of loading domain and unloading domain, which can be seen as 2 tensorial zones. With several plastic potentials, 4, 8, …tensorial zones can thus be defined. In each zone, the constitutive relation can be written as:

$$\underline{d\varepsilon} = \underline{\underline{N}} \cdot \underline{d\sigma} \tag{15}$$

using classical change of notations where tensors of second order become vectors of sixth order and fourth order tensor become a second order tensor. Matrix $\underline{\underline{N}}$ represents the tangent elasto-plastic tensor in the proper tensorial zone. Substituting relation *(15)* in equation *(13)*, potential instabilities arise when:

$$d^2W = 0 \Leftrightarrow \underline{d\sigma} \cdot \underline{\underline{N}} \cdot \underline{d\sigma} = 0 \Leftrightarrow \underline{d\sigma} \cdot \underline{\underline{N_s}} \cdot \underline{d\sigma} = 0 \tag{16}$$

which gives the following equation of the elliptical cone in the 3D space of principal stress rate ([26]):

$$\frac{d\sigma_1^2}{E_1}+\frac{d\sigma_2^2}{E_2}+\frac{d\sigma_3^2}{E_3}-\left(\frac{\nu_1^2}{E_1}+\frac{\nu_2^1}{E_2}\right)d\sigma_1 d\sigma_2-\left(\frac{\nu_3^2}{E_3}+\frac{\nu_2^3}{E_2}\right)d\sigma_2 d\sigma_3-\left(\frac{\nu_1^3}{E_1}+\frac{\nu_3^1}{E_3}\right)d\sigma_3 d\sigma_1=0 \tag{17}$$

where E_i are the generalized tangent Young's moduli and υ_i the generalized tangent Poisson's ratio.

Hence stability is conditioned by the loading direction or in other terms by the loading path. When Equation *(17)* has no solutions, $\underline{\underline{N_s}}$ is positive definite and no failure is possible. The stress state is said to be outside the bifurcation domain (there is not any unstable loading direction). Conversely, failures are possible along loading directions inside the cone. The stress state is said to be inside the bifurcation domain (there is at least one unstable loading direction or more generally an instability cone). Illustrations of the bifurcation domain limit according to the constitutive model of Darve are presented in Figure 10. Depending on the positiveness of $\underline{\underline{N_s}}$ eigenvalues, elliptical cone can degenerate into a simple straight line or into the intersection of two planes ([27]). Assuming that at the virgin state all eigenvalues are strictly positive and then they are evolving continuously with the loading parameter, limit of the bifurcation domain is given by the relationship:

$$\det\left(\underline{\underline{N_S}}\right)=0 \tag{18}$$

From a technical point of view, when $\det\left(\underline{\underline{N_S}}\right)$ vanishes for the first time in a tensorial zone it must be verified that the eigenvector associated with a zero eigenvalue belongs to this tensorial zone ([28]).

As mentioned above, inside the bifurcation domain, instability cones can develop ([26]). Here they are obtained using constitutive models provided by Darve ([29]) along a drained triaxial stress path as displayed in Figure 11.

Concerning the piece-wise linear model it can be noticed that elliptical cones have to be cut in their proper tensorial zone. As far as the incrementally non linear model is considered, this elliptical structure disappears.

5.2. Generalized failure rule, divergence instability

In this section, we will show that failure along loading paths whose current direction is inside the instability cone can be defined as a limit state similar to those provided by classical elastoplasticity theory, but this limit state is now a mixed one and the associated stress state is strictly inside this plasticity limit. To do so, we define stress proportional loading paths in the same way as the strain proportional tests presented in Section 2, as follows:

$$\begin{cases} d\sigma_1 = cst \quad cst \in \Re \\ d\sigma_1 + R d\sigma_3 = 0 \quad R \in \Re^* \\ d\sigma_2 - R' d\sigma_3 = 0 \quad R' \in \Re \end{cases} \tag{19}$$

$\Re$ denotes the real numbers and $\Re^*$ the real numbers but zero. For such loading paths it is possible to write the constitutive relation using the following form:

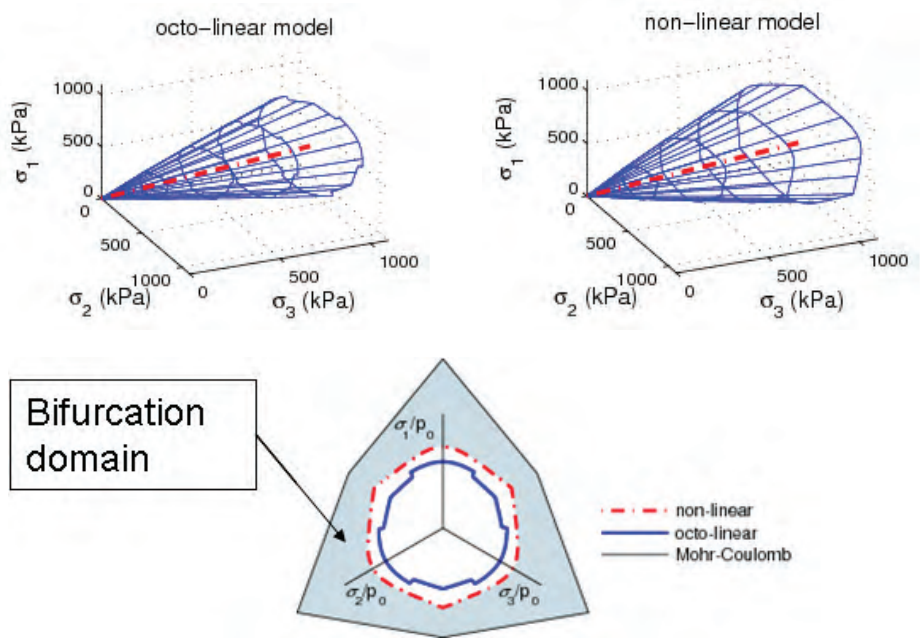

Figure 10. Bifurcation domain plotted with the octo and non-linear model of Darve for dense Hostun sand

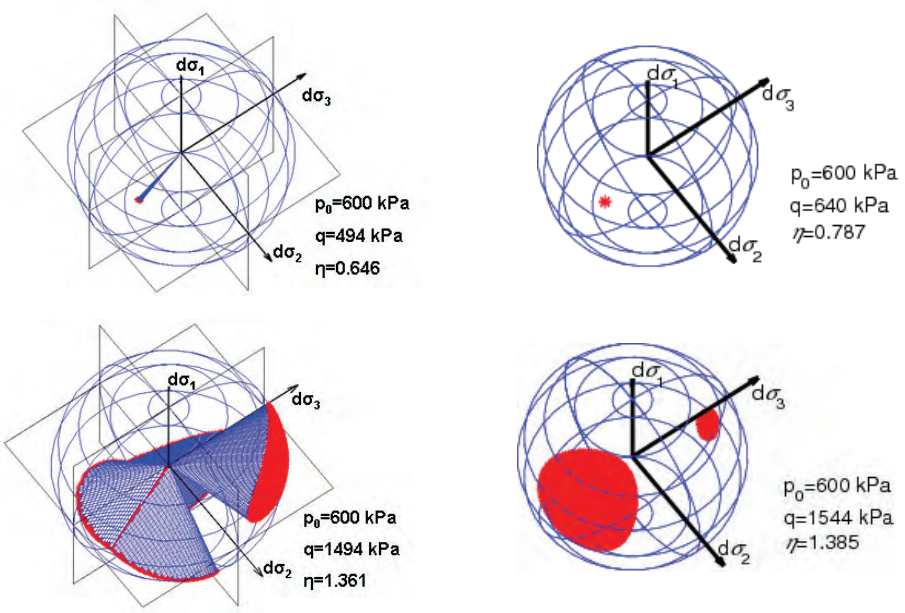

Figure 11. 3D cones for dense Hostun sand, on the left: octo-linear model, on the right: non-linear model

$$\begin{bmatrix} d\varepsilon_1 - \dfrac{d\varepsilon_3}{R} - \dfrac{R'}{R} d\varepsilon_2 \\ d\sigma_1 + R d\sigma_3 \\ d\sigma_2 - R' d\sigma_3 \end{bmatrix} = \underline{\underline{S}} \begin{bmatrix} d\sigma_1 \\ \dfrac{d\varepsilon_3}{R} + \dfrac{R'}{R} d\varepsilon_2 \\ d\varepsilon_2 \end{bmatrix} \tag{20}$$

R and *R'* allows the description of all loading directions. Then, for partCUlar values of *R* and *R'* which describe directions included in the instability cone, $\varepsilon_1 - \dfrac{\varepsilon_3}{R} - \dfrac{R'}{R}\varepsilon_2$ reaches an extreme. Hence, because of static constraint (Equation 18), at the $\varepsilon_1 - \dfrac{\varepsilon_3}{R} - \dfrac{R'}{R}\varepsilon_2$ peak, $\det\left(\underline{\underline{S}}\right)$ vanishes for non trivial solutions of Equation (20) and a generalized flow rule (a so-called "failure rule") can be defined. Furthermore, knowing that second order work can be rewritten as in Equation 21:

$$\left(d\varepsilon_1 - \frac{d\varepsilon_3}{R} - \frac{R'}{R} d\varepsilon_2\right) d\sigma_1 + \left(d\sigma_1 + R d\sigma_3\right)\left(\frac{d\varepsilon_3}{R} + \frac{R'}{R} d\varepsilon_2\right) + \left(d\sigma_2 - R' d\sigma_3\right) d\varepsilon_2$$

$$= d\sigma_1 d\varepsilon_1 + d\sigma_2 d\varepsilon_2 + d\sigma_3 d\varepsilon_3 = d^2 W \tag{21}$$

this quantity vanishes at this peak. That's why second order work criterion can be seen as a divergence instability criterion ([30]). Eventually, it has to be noticed that $\det\left(\underline{\underline{N_S}}\right)$ is not positive when $\det\left(\underline{\underline{S}}\right)$ vanishes and the stress state is inside the bifurcation domain. *R* and *R'* defines a loading direction inside an instability cone, and effective failure takes place only if mixed conjugated variables are controlled as presented in Equation *(20)*.

To illustrate this purpose, a drained triaxial path on a loose Hostun sand, followed by a loading path defined with *R'=1* and *R=0.85* has been simulated experimentally and numerically with incrementally non linear Darve's model ([24]). Response of this path is presented in Figures 10, 11 and 12 ([31]).

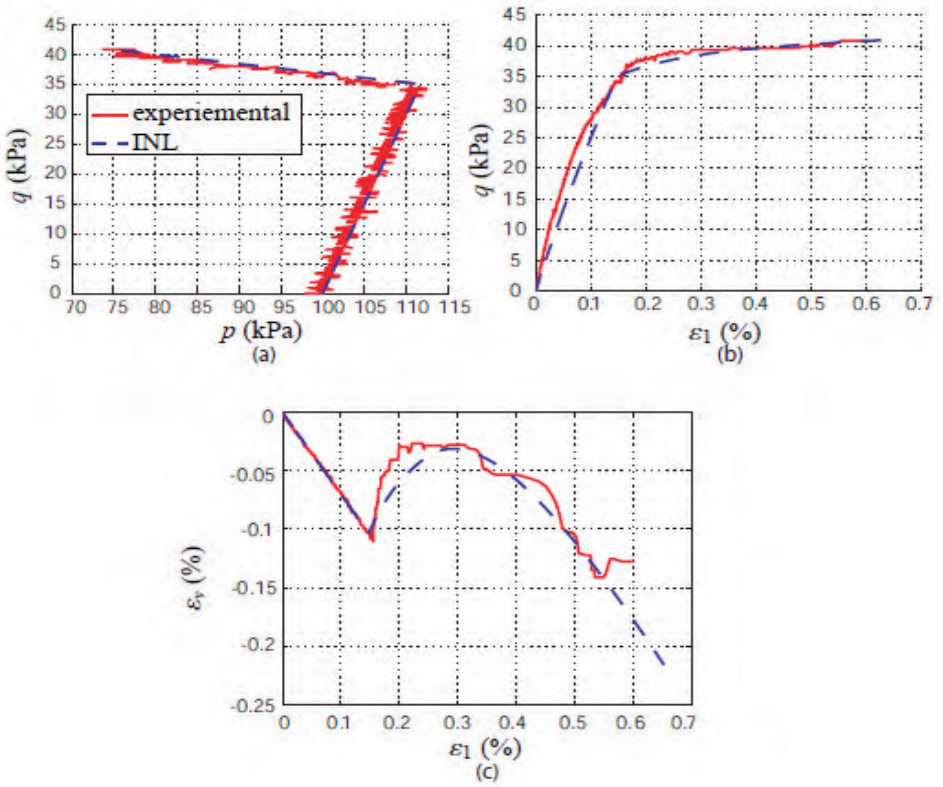

Figure 11. Response of the loading path given by *R=0.85* and *R'=1*. Before the stress proportional loading path, a drained triaxial compression has been applied allowing entry into the bifurcation domain. The experimental response is represented with the continuous line, whereas the response given by the incrementally non-linear Darve's model is displayed with the dashed line [31].

Numerically, it is convenient to illustrate the purpose exposed above with the help of the following Figures:

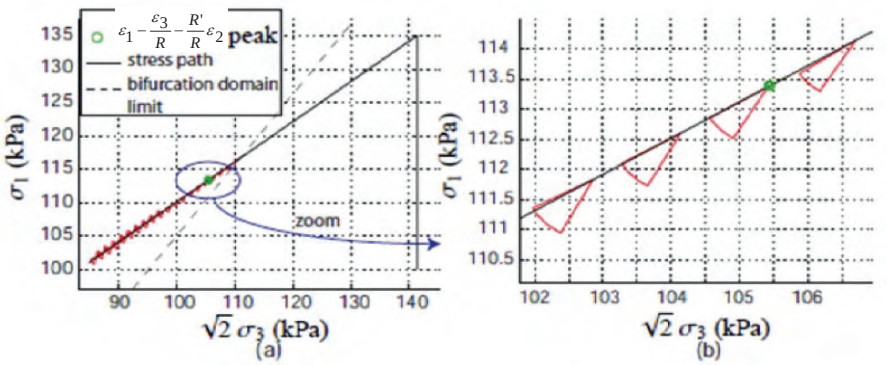

Figure 12. Instability cones along the considered loading path, with in dashed line the bifurcation domain limit and at the green point the occurrence of the $\varepsilon_1 - \frac{\varepsilon_3}{R} - \frac{R'}{R}\varepsilon_2$ peak.

It has to be noticed that the $\varepsilon_1 - \frac{\varepsilon_3}{R} - \frac{R'}{R}\varepsilon_2$ peak does not coincide with ε_v as it is the case for q constant shear tests. The following picture illustrates this fact:

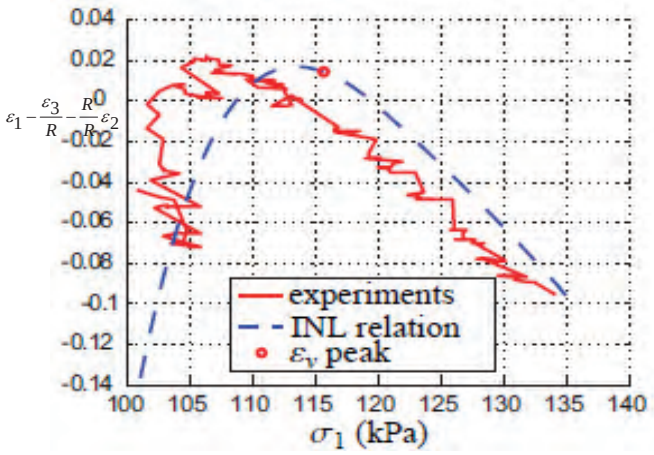

Figure 13. Generalised strain variations and occurrence of the first unstable direction at the strain peak according to the proportional stress path with *R'=1* and *R=0.85*. The volume variation peak is given by the circular point, which does not correspond to the generalized strain peak.

5.3. Withney-Umbrella graph

In this section we present critical values of the loading parameter for the constraints parameters *R* and *R'*. These kinds of graphs are derived from the so called Witney-Umbrella equation. In our case the canonical shape of this equation takes the following form:

$$\sigma_1 R^2 - R'^2 = 0 \tag{22}$$

which can be seen as a partCUlar case of Equation *(17)* by substituting static constraints from expression *(19)*. For linearized problems, the solution of this equation provides σ_1 critical as a function of the constraint parameters *R* and *R'*. However, in our case linearization is not possible, and because of the complexity of the constitutive model, no analytical solutions can be derived.
Hence, to plot this graph, by considering the incrementally non-linear constitutive model of Darve calibrated on dense Hostun sand, we have simulated a drained triaxial path. At each increment of $d\sigma_1$ we have investigated all loading paths defined by Equation *(19)* until it reaches or not a critical unstable state given by the second order work criterion. When such a critical state has been found, a point has been plotted in the 3D graph which gives σ_1 critical as a function of *R* and *R'*. Figure 14 displays these results. Even if the surface seems complicated, we retrieve one basic characteristic of classical surfaces found in linearized problems, i.e. the vertical axis corresponds to a singular line of the surface.

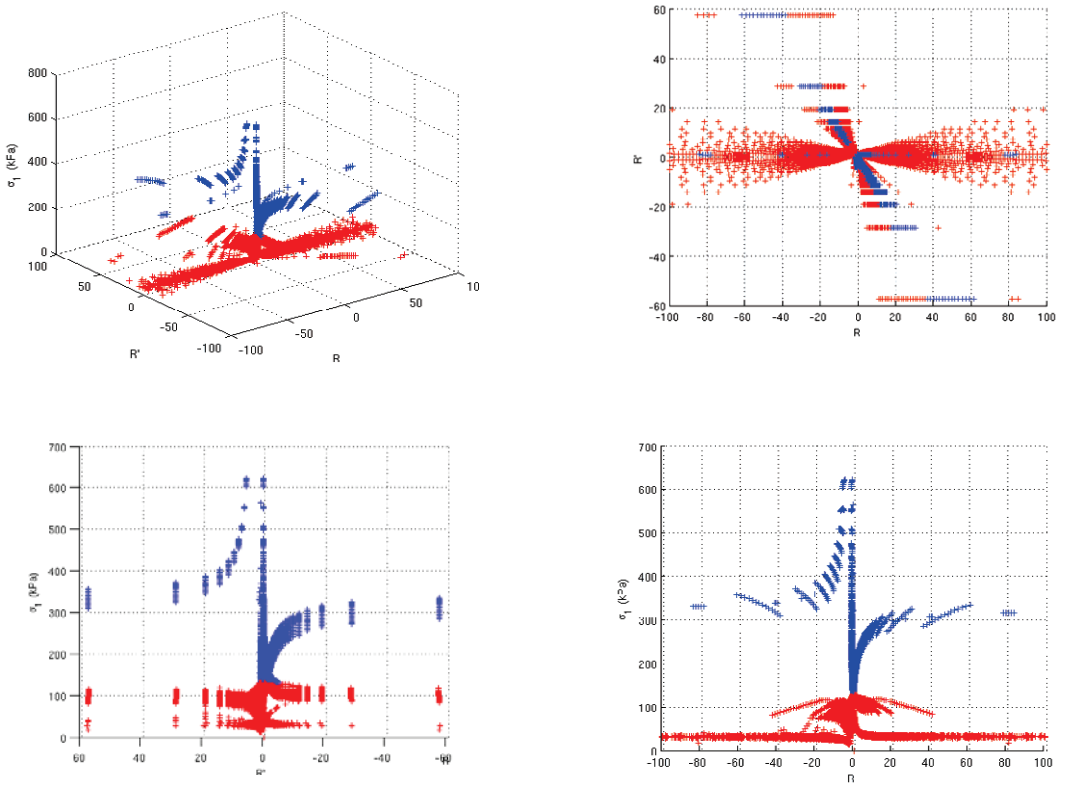

Figure 14. Critical load σ_1 as a function of *R* and *R'* parameters. Red points corresponds to critical load when $d\sigma1<0$ and blue ones when $d\sigma1>0$.

6. Conclusion

The question of failure, bifurcation and instability has been revisited in this paper in the case of granular media. These novel views are essentially due to the non-associate character of plastic strains for these materials, and, certainly, the obtained general trends can be generalized, from a qualitative point of view, to other non-associate elasto-plastic materials. Experimental results (Section 2), theoretical analysis (Section 3), discrete element computations (Section 4) and phenomenological developments (Section 5) have shown convergent viewpoints giving rise to a coherent framework to consider failure in geomaterials :

- There is a whole stress domain (and not only a single failure surface) where bifurcations, instabilities, losses of uniqueness and failures can appear. The limits of this domain (if we ignore flutter instabilities) are given by the vanishing values of the determinants respectively of the elasto-plastic matrix and its symmetric part,
- The necessary condition of divergence instability is given by the loss of positive definitiveness of the elasto-plastic matrix (the converse of the second order work sufficient condition of stability). Thus, inside the bifurcation domain, the matrix exhibits some “isotropic cones” (in the meaning of linear

algebra), which defines the “unstable stress directions” (from a mechanical viewpoint). Basically the second order work condition has a directional nature.

- Failure is generally associated with a sudden transition from a quasi-static regime to a dynamic one through a bifurcation state. This experimental evidence has been explained analytically by the link between the value of kinetic energy just after failure and the difference between the external applied second order work and the internal constitutive second order work. This relationship has been carefully examined and eventually verified by numerical simulations using a discrete element method.

These tools to analyze failure have been implemented in finite element softwares to solve boundary value problems such as landslides ([26], [32]).

References

[1] Vardoulakis I., Goldscheider M., Gudehus G. 1978. Formation of shear bands in sand bodies as a bifurcation problem. Int. J. Num. Anal. Meth. In Geomech., 2(2) : 99-128

[2] Khoa H.D.V., Georgopoulos I.O., Darve F., Laouafa F. 2006. Diffuse failure in geomaterials, experiments and modelling. Comp. and Geotech., 33: 1-14

[3] Bardet J.P., Numerical simulations of the incremental responses of idealized granular materials. *International Journal of Plasticity*, 1994; 10/8:879-908.

[4] Lanier J., Jean M., Experiments and numerical simulations with 2D disks assembly. *Powder Technology*, 2000; 109:206-221.

[5] Radjai F., Wolf D.E., Jean M., Moreau J.P., Bimodal character of stress transmission in granular packings. Physical Review Letters, 1998; 80/1:61-64

[6] Chu, J. Lo, S-C. R., and Lee, I. K. 1993. Instability of Granular Soils under Strain Path Testing. Journal of Geotechnical Engineering, Volume 119, Issue 5, pp. 874-892.

[7] Lancelot, L. Shahrour, I., and Al Mahmoud, M. 2004. Instability and Static Liquefaction on Proportional Strain Paths for Sand at Low Stresses, Journal of Engineering Mechanics, Volume 130, Issue 11, pp. 1365-1372.

[8] Sivathayalan, S., and Logeswaran, P. 2007. Behaviour of sands under generalized drainage boundary conditions. Canadian Geotechnical Journal, 44(2)(3): 138–150.

[9] Sivathayalan, S. and Logeswaran, P. 2008. Experimental assessment of the response of sands under shear–volume coupled deformation. Canadian Geotechnical Journal, 45(9)(10): 1310–1323.

[10] Darve, F. Sibille, L. Daouadji, A. and Nicot, F. 2007. Bifurcations in granular media: macro- and micro-mechanics approaches. Comptes Rendus Mécanique, 335:496-515.

[11] Daouadji, A. Al Gali, H. Darve, F. Zeghloul, A. 2010. Instability in Granular Materials: Experimental Evidence of Diffuse Mode of Failure for Loose Sands. Journal of Engineering Mechanics, Vol. 136, No. 5: 575-588.

[12] Daouadji, A. Darve, F. Al Gali, H. Hicher, P. Y. Laouafa, F. Lignon, S. Nicot, F. Nova, R. Pinheiro, M. Prunier, F. Sibille, L and Wan, R. 2010. Diffuse failure in geomaterials: Experiments, theory and modelling. International Journal for Numerical and Analytical Methods in Geomechanics, DOI: 10.1002/nag.975.

[13] Nova, R. 1994. Controllability of the incremental response of soil specimens subjected to arbitrary loading programmes. Journal of the Mechanical Behavior of Materials, 5(2)(3):193–201

[14] Darve, F. Servant, G. Laouafa, F. Khoa, H.D.V. 2004. Failure in geomaterials. Continuous and discrete analyses. Computer Methods in Applied Mechanics and Engineering, vol. 193, n 27-29, pp. 3057-3085.

[15] Nicot, F., and Darve, F. (2007): A micro-mechanical investigation of bifurcation in granular materials. Int. J. of Solids and Structures, Vol. 44, pp. 6630-6652.

[16] Nicot, F., Darve, F., and Khoa, H.D.V. (2007): Bifurcation and second-order work in geomaterials. Int. J. Num. Anal. Methods in Geomechanics, Vol. 31, pp. 1007-1032.

[17] Nicot, F., Sibille, L., and Darve, F. (2011): Failure as a bifurcation toward a dynamic regime. Int. Journal of Plasticity, *in press*.

[18] Cundall, P.A., and Strack, O.D.L. (1979): A discrete numerical model for granular assemblies. Géotechnique, Vol. 29, pp. 47-65.

[19] Love A.E.H. (1927): A Treatise of Mathematical Theory of Elasticity. Cambridge University Press, Cambridge, 1927.

[20] Weber J. (1966): Recherches concernant les contraintes intergranulaires dans les milieux pulvérulents. Bulletin de Liaison des Ponts-et-chaussées, No 20, pp. 1-20.

[21] Nicot, F., Sibille, L., and Darve, F. (2012): Failure in rate-independent granular materials as a bifurcation toward a dynamic regime. Int. Journal of Plasticity, Vol. 29, pp. 136–154.

[22] Sibille L, Nicot F., Donzé F.V. and Darve F. (2009): Analysis of failure occurrence from direct simulations. European Journal of Environnemental and Civil Engineering, Vol. 13, pp. 187-201
[23] Lade P V, Static instability and liquefaction of loose fine sandy slopes. *Journal of Geotechnical Engineering* 1992; **118/1**: 51–71.
[24] Laouafa F, Prunier F, Daouadji A, Al Gali H, Darve F, Stability in geomechanics, experimental and numerical analyses. *International Journal for Numerical and Analytical Methods in Geomechanics* 2011; **35/2**:112-139.
[25] Hill R, A general theory of uniqueness and stability in elasto-plastic solids. *Journal of the Mechanics and Physics of Solids* 1958;**6**:236–249.
[26] Prunier F, Nicot F, Darve F, Laouafa F, Lignon F, 3D multi scale bifurcation analysis of granular media. *Journal of Engineering Mechanics (ASCE)* 2009;**135/6**:493-509.
[27] Prunier F, Laouafa F, Darve F, 3D bifurcation analysis in geomaterials. Investigation of the second order work criterion. *European Journal of Environmental and civil Engineering* 2009;**13/2**:135-147.
[28] Prunier F, Laouafa F, Lignon S, Darve F, Bifurcation modeling in geomaterials:from the second order work criterion to spectral analyses. *International Journal for Numerical and Analytical Methods in Geomechanics* 2009;**33/9**:1169-1202.
[29] Darve F, Flavigny E, Meghachou M, Yield surfaces and principle of superposition revisited by incrementally non-linear constitutive relations. *International Journal of Plasticity* 1995;**11/8**:927–948.
[30] Nicot F, Challamel N, Lerbet J, Prunier F, Darve F, Bifurcation and generalized mixed loading conditions in geomaterials. *International Journal for Numerical and Analytical Methods in Geomechanics* 2010; **DOI**: 10.1002/nag.959.
[31] Laouafa F., Prunier F., Daoudji A., Al Gali H., Darve F., Satbility in geomechanics, experimental and numerical analyses. *Intenrational Journal for Numerical and Analytical Methods in Geomechanics*, 2011; 35/2:112-139
[32] Lignon S., Laouafa F.,Prunier F., Khoa H.D.V.,Darve F. 2009. Hydro-mechanical modelling of landslides with a material instability criterion , Geotechnique, 59(6): 513-524